ACS OMEGA

Open Access

http://pubs.acs.org/journal/acsodf

Article

Thermodynamic and Kinetic Studies of Mononuclear Non-Heme High-Valent $(FeO)^{2+}$ Complexes

Bao-Long Chen,* Jin-Ye Zhang,* Wen-Jie Xu, Sheng-Yi Yan, and Xiao-Qing Zhu*

Cite This: *ACS Omega* 2025, 10, 3718−3728

Read Online

ACCESS | Metrics & More | Article Recommendations | Supporting Information

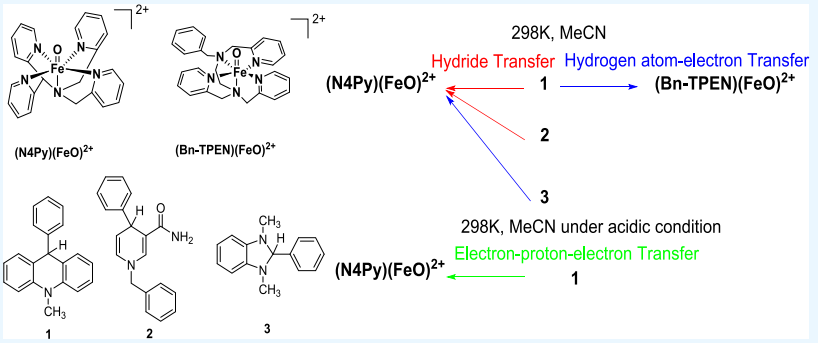

ABSTRACT: Mononuclear nonheme high-valent $(FeO)^{2+}$ complexes participate in many enzymatic oxidation−reduction cycles in a living body and play a key role in organic synthesis. The concept of molecular ID (molecular identities) was proposed and applied in our previous work; it covers all thermodynamic data for compounds containing an active carbon−hydrogen bond: oxidation potential, hydride anion affinity, proton affinity, and hydrogen atom affinity. To facilitate quantitative analysis of the physical organic chemistry and molecular biology properties of $(FeO)^{2+}$ complexes, the molecular identities and reaction thermodynamic platform of representative complexes were established based on the thermodynamic data, such as $(N4Py)(FeO)^{2+}$ and $(Bn\text{-}TPEN)(FeO)^{2+}$, and their kinetic characteristics. Finally, the findings of this study are as follows: first, the reaction between $(N4Py)(FeO)^{2+}$ and hydride donors **1**/**2** (Scheme 1) followed a one-step hydride anion transfer mechanism. The reactions between $(N4Py)(FeO)^{2+}$ and hydride donors **3** (Scheme 1) and between $(Bn\text{-}TPEN)(FeO)^{2+}$ and hydride donors **1** followed the hydrogen atom−electron transfer mechanism. Second, by comparison of high-valent $(RuO)^{2+}$ complexes and organic hydride acceptors, the essential laws in selecting the reaction mechanism were obtained to determine the reaction mechanism of this study. Third, the reaction between $(N4Py)(FeO)^{2+}$ and **1** followed the electron−proton−electron transfer mechanism under acidic conditions.

1. INTRODUCTION

Mononuclear heme and nonheme iron enzymes, crucial for metabolism, hypoxia treatment, DNA repair, and biodegradation, are vital components in natural products and anticancer drugs.[1,2] Specifically, the mononuclear nonheme Fe enzyme, a major catalyst for activating O_2 in a living body, extensively participates in oxidation−reduction reactions in metabolism, such as the prolyl hydroxylase and halogenase CytC3-catalyzed cycles and α-ketoglutarate oxidase TauD. The mononuclear nonheme Fe enzyme can oxidize various substrates, including triphenylphosphine, thiol, N,N-dialkyl amine, aromatic hydrocarbons, alkyl aromatic compounds, olefin, alcohol, and alkane, using oxygen atom transfer.[3−17] These reactions provide an experimental foundation for simulating studies of nonheme enzymes.

Owing to the weak chemical stability of the $(FeO)^{2+}$ complex,[18] it and its reaction intermediate cannot be captured easily. Therefore, a method to quantitatively evaluate its chemical properties is required. Generally, it is defined that when a carbonyl C═O receives a hydride ion, it generates the enthalpy of the corresponding alcohol anion, resulting in the hydride affinity of an aldehyde or ketone. Owing to its strong oxidizing properties, the $(FeO)^{2+}$ complex differs from aldehydes, ketones, imines, and other compounds with unsaturated double bonds. As shown in Scheme 1, the molecular identities (molecular IDs)[19] of representative $(FeO)^{2+}$ complexes, such as $(N4Py)(FeO)^{2+}$ and $(Bn\text{-}TPEN)(FeO)^{2+}$, were established. The reaction mechanisms between $(N4Py)(FeO)^{2+}$ and **1**/**2**/**3**, and between $(Bn\text{-}TPEN)(FeO)^{2+}$ and **1** were all inferred, respectively, to understand if the hydride donors with different hydride-donating capacities had the same reaction mechanism with the $(FeO)^{2+}$ complex. All kinetic and

Received: September 30, 2024
Revised: January 2, 2025
Accepted: January 9, 2025
Published: January 27, 2025

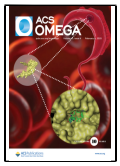

Scheme 1. Compounds Synthesized in this Study.[a]

Hydride Acceptor:

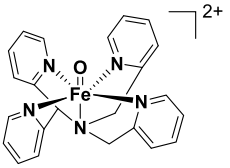

$(N4Py)(FeO)^{2+}$

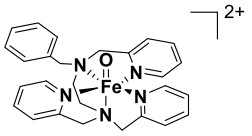

$(Bn\text{-}TPEN)(FeO)^{2+}$

Hydride Donor:

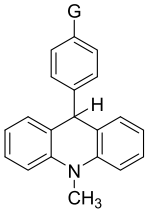

1

1a(H),1b(CH_3),1c(OCH_3), 1d(F),1e(Cl),1f(CF_3)

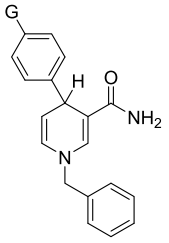

2

2a(H),2b(CH_3),2c(OCH_3), 2d(Cl),2e(CF_3)

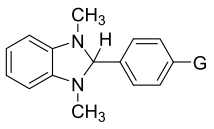

3

3a(H),3b(CH_3),3c(OCH_3), 3d(F),3e(Cl),3f(CF_3),3g(NO_2), 3h(CN),3i(NMe_2)

[a]G represents the substituted group

Scheme 2. Representative Hydride Transfer Reactions in this Study

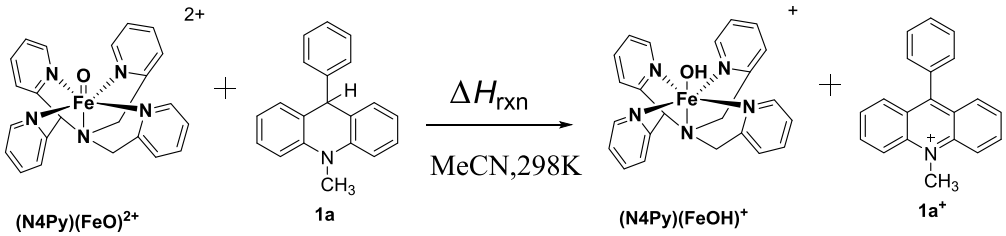

$(N4Py)(FeO)^{2+}$ + **1a** → $(N4Py)(FeOH)^{+}$ + $\mathbf{1a}^{+}$

thermodynamic experiments in this study were conducted in acetonitrile at 298 K.

The hydride ion can exist only in such a state in the gas phase. The thermodynamic driving force of hydride transfer depends on the capacity of the hydride donor to provide the hydride and the capacity of the hydride acceptor to abstract the hydride, and the process of $(FeO)^{2+}$ complexes abstracting the hydride anion is exactly opposite to the heterolytic process of anions (eq 1). Therefore, the hydride affinity in the solution ($\Delta H_{H}^{-}{}_{A}$) can be obtained from the reaction enthalpy change of the corresponding hydride acceptor with a suitable hydride donor such as **1a**, as shown in Eq 2 and Scheme 2. Correspondingly, $\Delta H_{H}^{-}{}_{D}$ stands for the hydride-donating enthalpy change.

$$\Delta H_{H-A}(N4Py)(FeO)^{2+} = -\Delta H_{H-D}(N4Py)Fe(OH)^{+} \quad (1)$$

$$\Delta H_{rxn} = \Delta H_{H-A}(N4Py)(FeO)^{2+} + \Delta H_{H-D}(\mathbf{1a}) \quad (2)$$

Strictly, the hydrogen element that moves from donor site to the acceptor site in any reaction is a hydrogen atom in condensed phases, which may be polarized negatively or positively according to the electronegativity of the atom to which it is bonded. The same holds for the hydrogen element of **1**, **2**, and **3**. To simplify the concept without violating scientific principles, the hydrogen transfer process (Scheme 3) of the $(FeO)^{2+}$ complexes primarily involves the following bond energy changes:

Scheme 3. Three Thermodynamic Cycles Constructed Based on the Chemical Process of $(FeO)^{2+}$ Complexes Abstracting Hydride Anion in Acetonitrile at 298 K

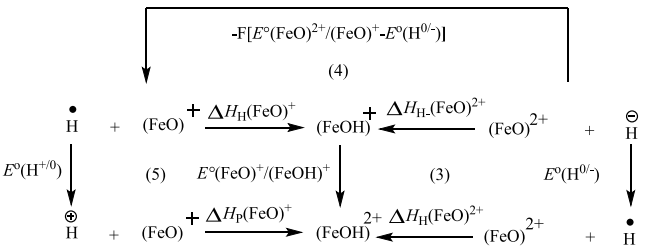

Hydrogen-atom affinity: $\Delta H_{H}(FeO)^{+}$ and $\Delta H_{H}(FeO)^{2+}$ are defined as the molar enthalpy changes of $(FeO)^{+}$ and $(FeO)^{2+}$ abstracting a hydrogen atom, respectively. Hydride affinity: $\Delta H_{H}^{-}(FeO)^{2+}$ is the molar enthalpy change of $(FeO)^{2+}$ abstracting a hydride anion. Proton affinity: $\Delta H_{P}(FeO)^{+}$ is defined as the molar enthalpy change of $(FeO)^{2+}$ abstracting a proton.

The thermodynamic parameters of reactants and reaction intermediates in Scheme 3 can be determined based on

https://doi.org/10.1021/acsomega.4c08847
ACS Omega 2025, 10, 3718−3728

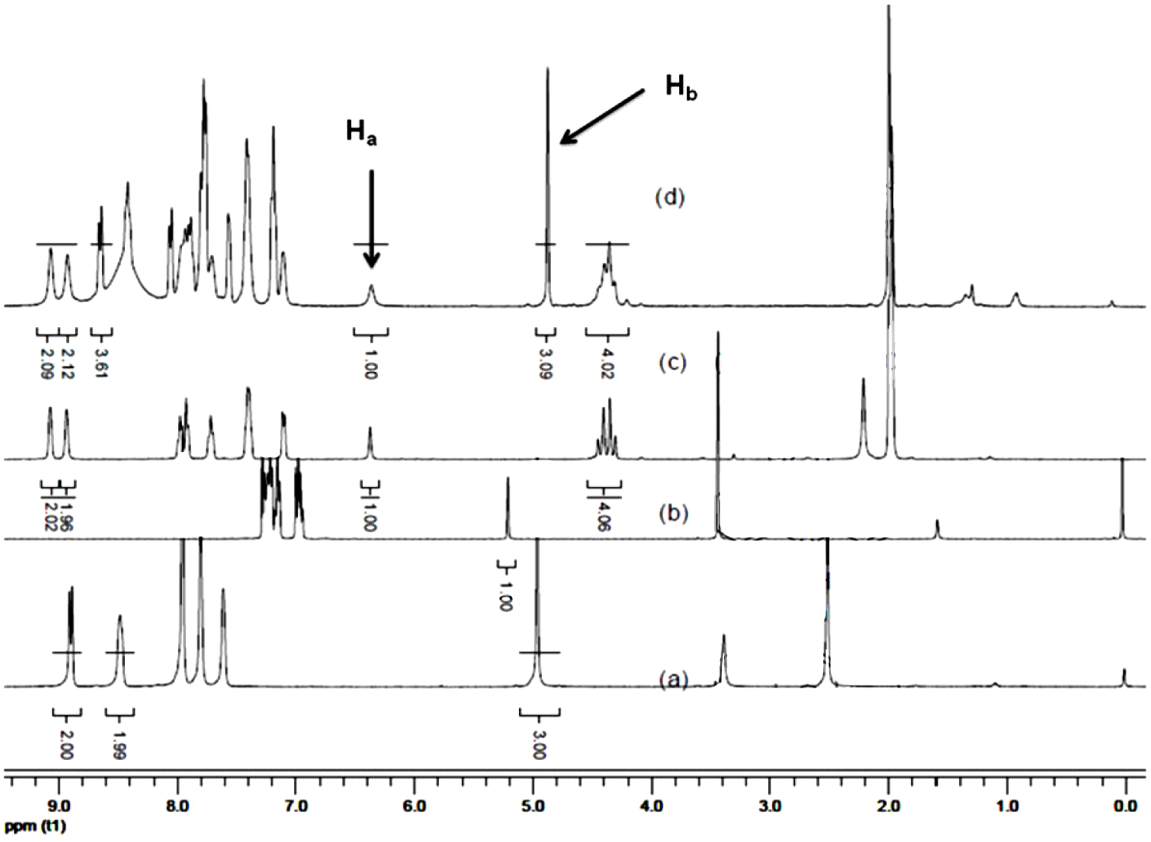

Figure 1. ^{1}H NMR spectra for the reaction products of (a) **1a**$^{+}$, (b) **1a**, (c) (N4Py)(FeOH)$^{+}$(CH_3CN), and (d) **1a** (39.1 mM) and (N4Py)(FeO)$^{2+}$(ClO_4)$_2$ (39.1 mM) in CD_3CN (0.5 mL). Correspondingly, H_a represents the characteristic hydrogen atom of (N4Py)-(FeOH)$^{+}$(CH_3CN), and H_b represents the characteristic hydrogen atom of **1a**$^{+}$.

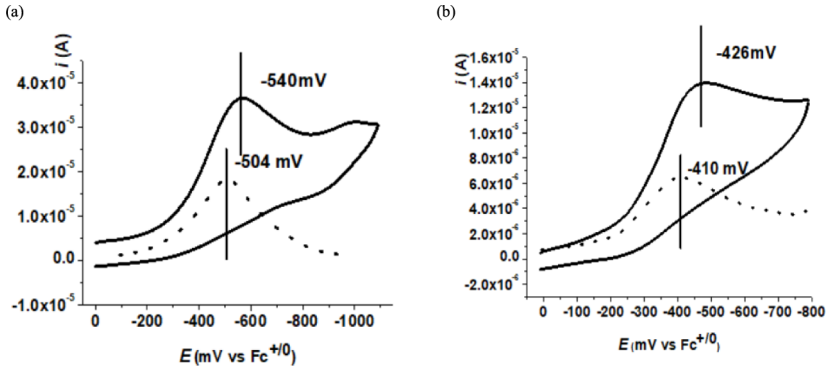

Figure 2. CV (solid lines) and OSWV (dashed lines) graphs of (a) (N4Py)(FeO)$^{2+}$(ClO_4)$_2$ (1 mM) and (b) (Bn-TPEN)(FeO)$^{2+}$(OTf)$_2$ (1 mM) in deaerated acetonitrile containing 0.1 M *n*-Bu_4NPF_6 as the supporting electrolyte. CV rate: 0.1 V/s. A standard three-electrode cell consists of a glassy carbon disk as work electrode, a platinum wire as a counter electrode, and 0.1 M $AgNO_3$/Ag (in 0.1 M *n*-Bu_4NPF^{6-} acetonitrile) as reference electrode.

electrochemical and calorimetric data, and eqs 3−5 provide the corresponding derivation equations. $E°(FeO)^{+}/(FeOH)^{+}$ represents the oxidation potential of $(FeOH)^{+}$ complexes, and $E°(FeO)^{2+}/(FeO)^{+}$ is the reduction potential of $(FeO)^{2+}$ complexes. ΔH is replaced with ΔG_{ET} and $E_{1/2}(H^{+/0})$ = −2.307 V (vs $Fc^{+/0}$), and $E_{1/2}(H^{0/-})$ = −1.137 V (vs $Fc^{+/0}$) with Fc representing ferrocene, taken with reference to values in the literature[20] for determining reversible potentials. F represents Faraday's constant (23.05 kcal mol^{-1} V^{-1}).

$$\Delta H_H(FeO)^{2+} = \Delta H_H^{-}(FeO)^{2+} + F[E°(FeO)^{+}/(FeOH)^{+} - E°(H^{0/-})] \quad (3)$$

$$\Delta H_H(FeO)^{+} = \Delta H_H^{-}(FeO)^{2+} + F[E°(FeO)^{2+}/(FeO)^{+} - E°(H^{0/-})] \quad (4)$$

$$\Delta H_p(FeO)^{+} = \Delta H_H(FeO)^{+} + F[E°(FeO)^{+}/(FeOH)^{+} - E°(H^{+/0})] \quad (5)$$

2. RESULTS

The proton nuclear magnetic resonance (^{1}H NMR) spectra of the $(FeO)^{2+}$ complexes were obtained, as shown in Figure 1. First, **1a** (39.1 mM) and (N4Py)$(FeO)^{2+}$ (39.1 mM) were dissolved in 0.5 mL of deuteroacetonitrile. After an hour of

https://doi.org/10.1021/acsomega.4c08847
ACS Omega 2025, 10, 3718−3728

dissolution, the characteristic hydrogen atom of $\mathbf{1a}^+$ (H_b, δ: 3H, 4.88, CH_3) was almost three times higher than that of $(N4Py)(FeOH)^+(CH_3CN)$ (H_a, δ: 1H, 6.36, CH), indicating a 1:1 stoichiometry between $(N4Py)(FeO)^{2+}$ and **1a**. The reaction process is shown in Scheme 2. A similar experiment was conducted between **1a** and $(Bn\text{-}TPEN)(FeO)^{2+}$, as shown in the Supporting Information, further confirming a 1:1 stoichiometry.

Furthermore, the thermodynamic data were acquired first using the common electrochemical measurement methods, including cyclic voltammetry (CV) and Osteryoung square wave voltammetry (OSWV) (Figure 2, Table 1, and Supporting Information).

Table 1. Reaction Heat (ΔH_r) of $(N4Py)(FeO)^{2+}(ClO_4)_2$ and $(Bn\text{-}TPEN)(FeO)^{2+}(OTf)_2$ with 3a in Acetonitrile at 298 K and the Corresponding Redox Potentials using CV and OSWV

		$E_{red}(L)(FeO)^{2+}$ [b]	$E_{ox}(L)(FeOH)^{+}$ [b]
$(L)(FeO)^{2+}$	ΔH_r [a]	OSWV	OSWV
N4Py	−73.5	−0.504	0.703
Bn-TPEN	−80.9	−0.410	0.410

[a] ΔH_r was obtained from ΔH_{rxn} of eq 2 by switching the sign, and ΔH_{rxn} was determined using titration calorimetry in acetonitrile at 298 K. The data, presented in kcal/mol, were the average values of at least three independent runs. The reproducibility was ≤0.5 kcal/mol. [b] Measured using OSWV in acetonitrile at 298 K, the units were in volts vs $Fc^{0/+}$ and were reproducible to 5 mV or better.

The CV measurement method can be replaced with DPV (differential pulse voltammetry). For the theoretical basis of electrochemical measurements, please refer to previous research.[21] In fact, it would be reasonable to estimate the standard potential of these complexes using the inflection point (approximately 0.5−0.66 of the peak current potential).[22]

The molar enthalpy change of the reaction in acetonitrile at 298 K (ΔH_{rxn}), as shown in eq 2, could be determined using titration calorimetry. First, the ΔH_{rxn} of the reaction between $(N4Py)(FeO)^{2+}$ and a suitable hydride donor **3a** was directly determined using isothermal titration calorimetry (ITC) (Figure 3). The previous work of the authors calibrated the hydride affinity of **3a**, denoted as ΔH_{H-D} (**3a**), to 54.1 kcal/mol.[23] ΔH_{rxn} of the reaction between $(Bn\text{-}TPEN)(FeO)^{2+}$ and **3a** was determined, and the relevant data are listed in Table 1.

Based on the electrochemical data $E_{1/2}(H^{+/0})$, $E_{1/2}(H^{0/-})$, and $\Delta H_{H^-A}(FeO)^{2+}$, the thermodynamic data were substituted into eqs 3−5 to obtain the hydrogen-atom affinity ($\Delta H_{HA}(X^+)^b$) of the $(FeO)^{2+}$ complexes and the hydrogen-atom affinity ($\Delta H_{HA}(X^{\bullet+})$) and proton affinity ($\Delta H_{PA}(X^{\bullet+})$) of the corresponding radical anions. The data are summarized in Table 2.

Table 2. Enthalpy Changes of $(L)(FeO)^{2+}$ (L = N4Py and Bn-TPEN)(X^+) Abstracting a Hydride or Hydrogen Atom and the Corresponding One-Electron Reductive Product $(L)(FeO)^+(X^{\cdot+})$ Abstracting a Proton or Hydrogen Atom in Acetonitrile at 298 K

$(L)(FeO)^{2+}$	$\Delta H_{H^-A}(X^+)$ [a]	$\Delta H_{HA}(X^+)$ [b]	$\Delta H_{PA}(X^{\cdot+})$ [b]	$\Delta H_{HA}(X^{\cdot+})$ [b]
N4Py	−127.6	−85.2	−43.6	−113.0
Bn-TPEN	−135.0	−99.5	−56.0	−118.4

[a] ΔH_{H^-A} (X^+) of N4Py and Bn-TPEN were estimated using eq 2. [b] $\Delta H_{H^-A}(X^+)$, $\Delta H_{PA}(X^{\cdot+})$, and $\Delta H_{HA}(X^{\cdot+})$ were estimated using eqs 3−5, respectively. The redox potentials of XH and X^+ were measured using the OSWV method, and $E_{red}(L)(FeO)^{2+}$ and $E_{ox}(L)(FeOH)^+$ were selected as they were closer to the corresponding standard redox potentials than the CV values in this study.

Furthermore, kinetic data were acquired. The obtained ultraviolet−visible (UV−vis) absorption spectra of $(FeO)^{2+}$ complexes and the organic hydride donors are shown in Figure 4, where the UV−vis peaks did not overlap; therefore, kinetic tests, as shown in Figure 5, were conducted. The detailed process is described in the Supporting Information. The dependence of k_{obs} on hydride donor concentration confirms

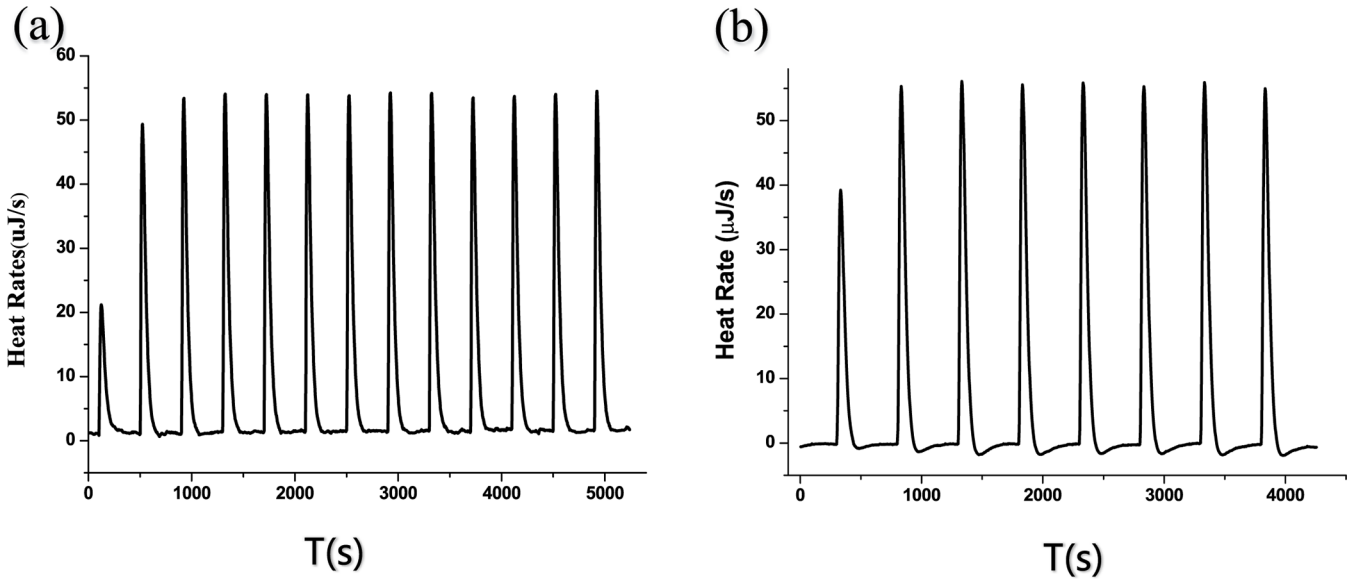

Figure 3. (a) ΔH_{rxn} of $(N4Py)(FeO)^{2+}$ with **3a** in anhydrous acetonitrile at 298 K. $(N4Py)(FeO)^{2+}$ (10 μL, 1.02 mM) was added to acetonitrile containing **3a** (10 mM) every 400 s for titration. (b) ΔH_{rxn} of $(Bn\text{-}TPEN)(FeO)^{2+}$ with **3a** in anhydrous acetonitrile at 298 K. $(Bn\text{-}TPEN)(FeO)^{2+}$ (10 μL, 0.97 mM) was added to acetonitrile containing **3a** (10 mM) every 500 s for titration.

https://doi.org/10.1021/acsomega.4c08847
ACS Omega 2025, 10, 3718−3728

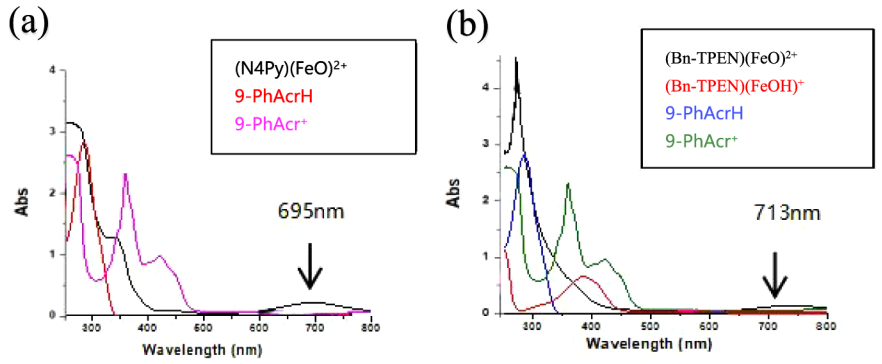

Figure 4. (a) UV−vis absorption spectra of $(N4Py)(FeO)^{2+}(ClO_4)_2$, 9-PhAcrH, and 9-PhAcr$^+$. (b) UV−vis absorption spectra of (Bn-TPEN)$(FeO)^{2+}(OTf)_2$, (Bn-TPEN)$(FeOH)^+(OTf)$, 9-PhAcrH, and 9-PhAcr$^+$. The concentration of all compounds was 0.1 mM.

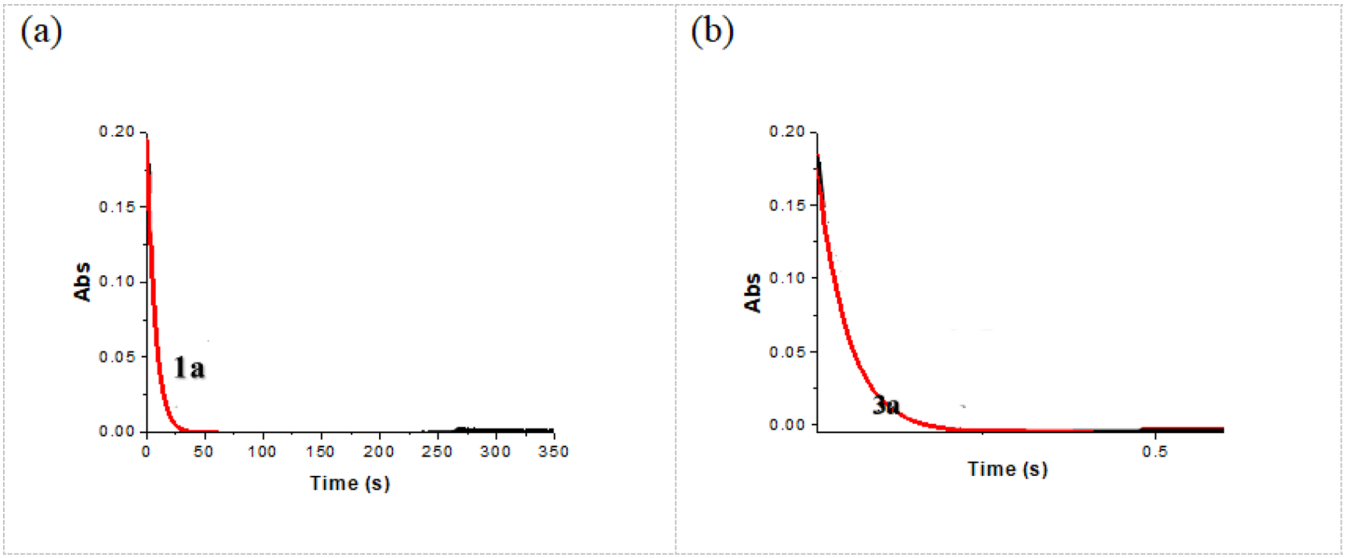

Figure 5. Time profiles of absorbance variations at 695 nm for the reaction of (a) **1a** and (b) **3a** with $(N4Py)(FeO)^{2+}$ at 298 K in acetonitrile under anaerobic conditions. $[(L)(FeO)]^{2+}]_0 = 0.96 \times 10^{-3}$ M.

that the reaction is a first-order reaction (Table 3 and Figure 6). As shown in Figure 7, a linear correlation between the second-order rate constant k_2 and the thermodynamic driving force was plotted to infer the hydride transfer reaction mechanisms.

Table 3. Enthalpy Changes of $(L)(FeO)^{2+}$ (L = (N4Py) and (Bn-TPEN) Abstracting a Hydride or Hydrogen Atom and the Corresponding One-Electron Reductive Product $[(L)(FeO)]^+(X^{\bullet+})$ Abstracting a Proton or Hydrogen Atom in Acetonitrile at 298 K

$(N4Py)(FeO)^{2+}$[a]	10 mM	20 mM	30 mM	40 mM	50 mM
k_{obs}[b]	0.3277	0.332	0.3363	0.3406	0.3449

[a]Measured using a stopped-flow spectrophotometer in acetonitrile at 298 K. [b]k_{obs} is the apparent rate constant and the unit is s^{-1}.

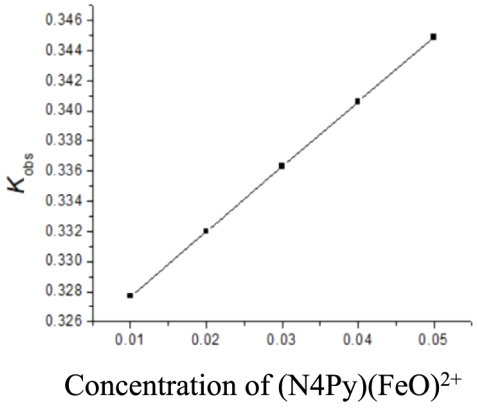

Figure 6. Dependence of k_{obs} on the concentration of $(N4Py)(FeO)^{2+}$.Time profiles of absorbance changes were created at 695 nm for the reaction of **1a** with $(N4Py)(FeO)^{2+}$ at 298 K in acetonitrile under anaerobic conditions. Concentration of $(N4Py)(FeO)^{2+} = 10 \times 10^{-3}$ M, 20×10^{-3} M, 30×10^{-3} M, 40×10^{-3} M, 50×10^{-3} M.

3. DISCUSSION

(1) How can the reaction mechanisms between the $(FeO)^{2+}$ complexes and organic hydride compounds be inferred, and how many reaction mechanisms are there?

According to the electrochemical and ITC data, the molecular IDs of $(N4Py)(FeO)^{2+}$ shown in Schemes 4 and 5 and (Bn-TPEN)$(FeO)^{2+}$ shown in the Supporting Information were obtained. The molecular IDs of $\mathbf{1}^+$, $\mathbf{2}^+$, and $\mathbf{3}^+$ were listed in the previous work[23−25] of the authors. These authors used electrochemical and thermodynamic measurements exactly as in this paper. However, the hydride donor of thermodynamic

https://doi.org/10.1021/acsomega.4c08847
ACS Omega 2025, 10, 3718−3728

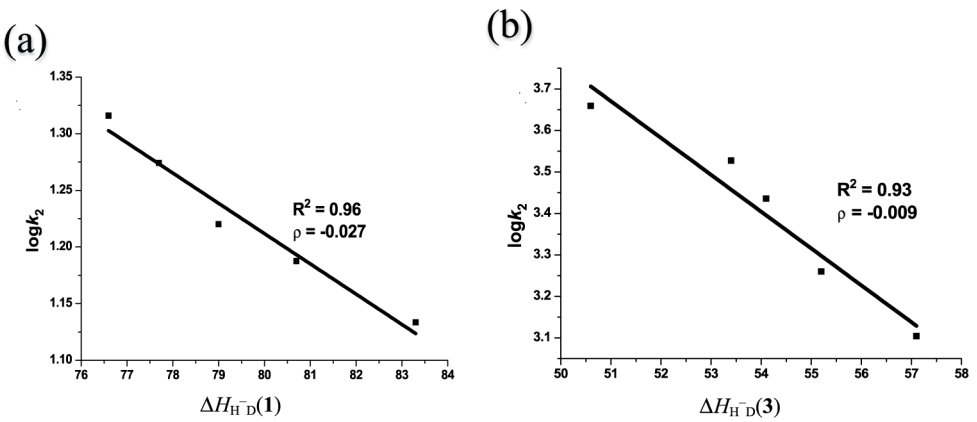

Figure 7. Plot of $\ln(k_2)$ against heterolytic bond dissociation energies (a) $\Delta H_{H^-D}(\mathbf{1})$ for the hydride transfer reaction of $(N4Py)(FeO)^{2+}$ with **1** in acetonitrile at 298 K and (b) $\Delta H_{H^-D}(\mathbf{3})$ for the hydride transfer reaction of $(N4Py)(FeO)^{2+}$ with **3a** in acetonitrile at 298 K. k_2 is the second-order rate constant.

Scheme 4. Thermodynamic Analytic Platform for the Hydride Transfer from 1a to $(N4Py)(FeO)^{2+}$

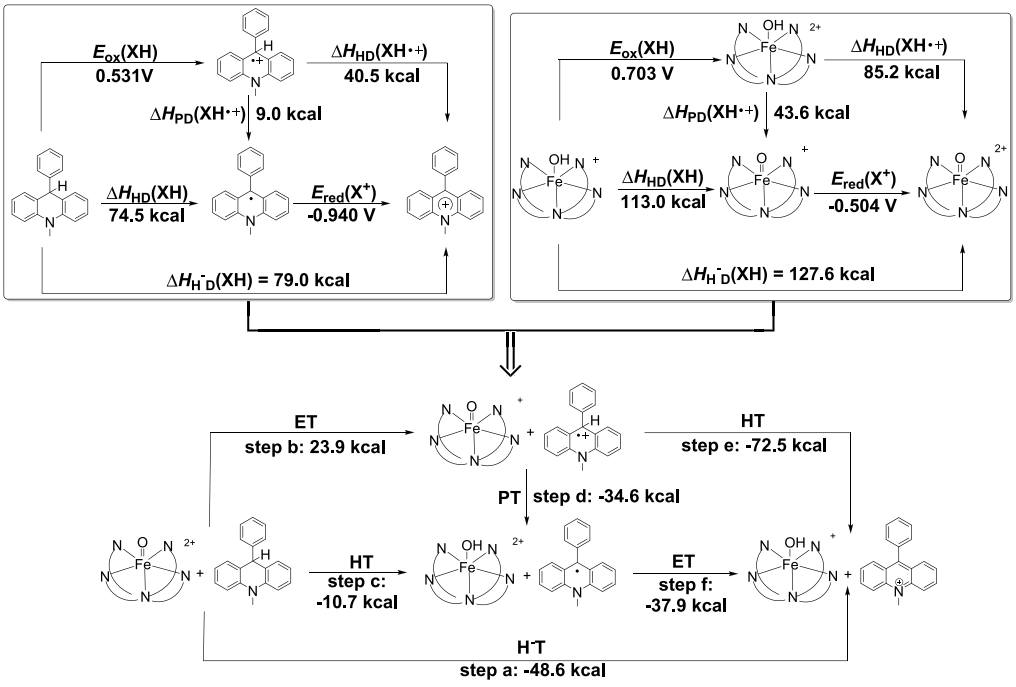

measurements was different. The molecular IDs of **1**, **2**, and **3** and the molecular IDs of the corresponding cations are also exactly the same.

Subsequently, the corresponding thermodynamic platforms were established.

The reaction mechanism between $(N4Py)(FeO)^{2+}$ and **1** is as follows:

According to Cheng's reserach[26] multistep reactions such as e^-−H and e^-−H^+−e^- reactions were excluded owing to the impossible thermodynamic prohibition of reactions when the enthalpy change of electron transfer exceeded 23.06 kcal/mol, as shown in Figure 8a. However, this thermodynamic prohibition value still needs to be confirmed or judged by theoretical chemists. The one-step hydride ion transfer had a much lower state energy change of −48.6 kcal/mol compared to hydrogen-atom transfer (−10.7 kcal/mol), favoring its consideration from the perspective of the thermodynamic driving force. Consequently, it complied with the hydride anion transfer mechanism. O_2 did not affect the reaction rate, indicating that no free radical was generated in this reaction. Hence, hydrogen-atom transfer was excluded, and the reaction mechanism between $(N4Py)(FeO)^{2+}$ and **1** was a one-step hydride transfer.

This reaction mechanism between $(N4Py)(FeO)^{2+}$ and **2** was inferred to be similar to that between $(N4Py)(FeO)^{2+}$ and **1**, and it was a one-step hydride transfer.

The reaction mechanism between $(N4Py)(FeO)^{2+}$ and **3** is as follows.

This reaction could not be an electron transfer step. However, the state energy change of electron transfer at the initiation step may be lower than that of the transient state. As shown in Figure 7b, the reaction rate decreased with the increased electron-withdrawing character of the substituent group, denoting that positive charges accumulated in the reaction center, and the rate-determining step could not be the proton transfer. Consequently, the electron−proton−electron transfer was excluded from this reaction. The subsequent hydrogen-atom transfer

https://doi.org/10.1021/acsomega.4c08847
ACS Omega 2025, 10, 3718−3728

Scheme 5. Thermodynamic Analytic Platform for the Hydride Transfer from 3a to $(N4Py)(FeO)^{2+}$

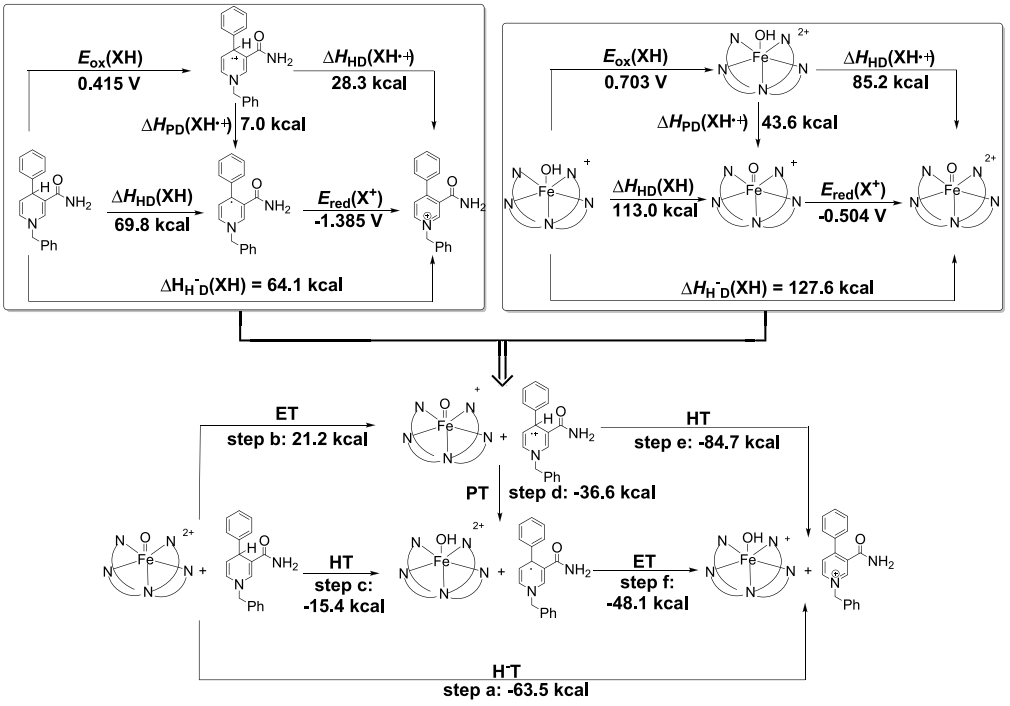

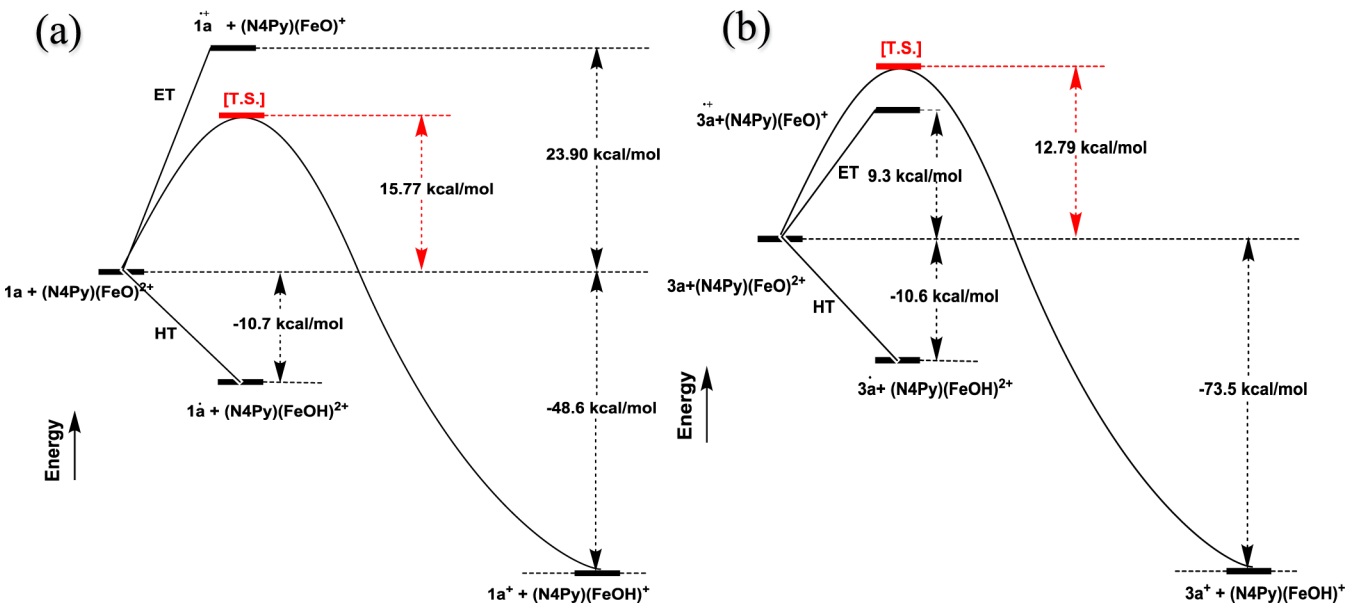

Figure 8. Comparison of state energy changes for the three possible initial steps with the activation free energy of hydride transfer reaction between (a) $(N4Py)(FeO)^{2+}$ and **1a** and (b) $(N4Py)(FeO)^{2+}$ and **3a**.

could be the rate-determining step if the reaction followed an electron−hydrogen atom transfer mechanism. However, the hydrogen-atom transfer had a highly negative thermodynamic driving force, which was inconsistent with the law of thermodynamics, thus excluding this hypothesis. Furthermore, as shown in Figure 6, the gradient (ρ) of the reaction rate constant between $(N4Py)(FeO)^{2+}$ and **3** changed less with the substituent group constant, agreeing with the reaction mechanism with hydrogen-atom transfer as the rate-determining step. Therefore, the reaction mechanism between $(N4Py)(FeO)^{2+}$ and **3** was hydrogen atom−electron transfer (Figure 8b).

Similar to the reaction mechanism between $(N4Py)(FeO)^{2+}$ and **3**, the reaction mechanism between $(Bn\text{-}TPEN)(FeO)^{2+}$ and **1** was inferred as hydrogen atom−electron transfer.

(2) Is it feasible to judge the reaction mechanism based only on thermodynamic factors? What are the internal factors affecting the reaction mechanism?

First, a comparison with Sheng-Yi Yan's study[27] on the reaction mechanism between Ru^{IV} and an organic hydride compound showed that a one-step hydride reaction and hydrogen atom−electron transfer were involved in the reaction between a metal carbonyl complex and an organic hydride compound, regardless of whether the enthalpy change in the

https://doi.org/10.1021/acsomega.4c08847
ACS Omega 2025, 10, 3718−3728

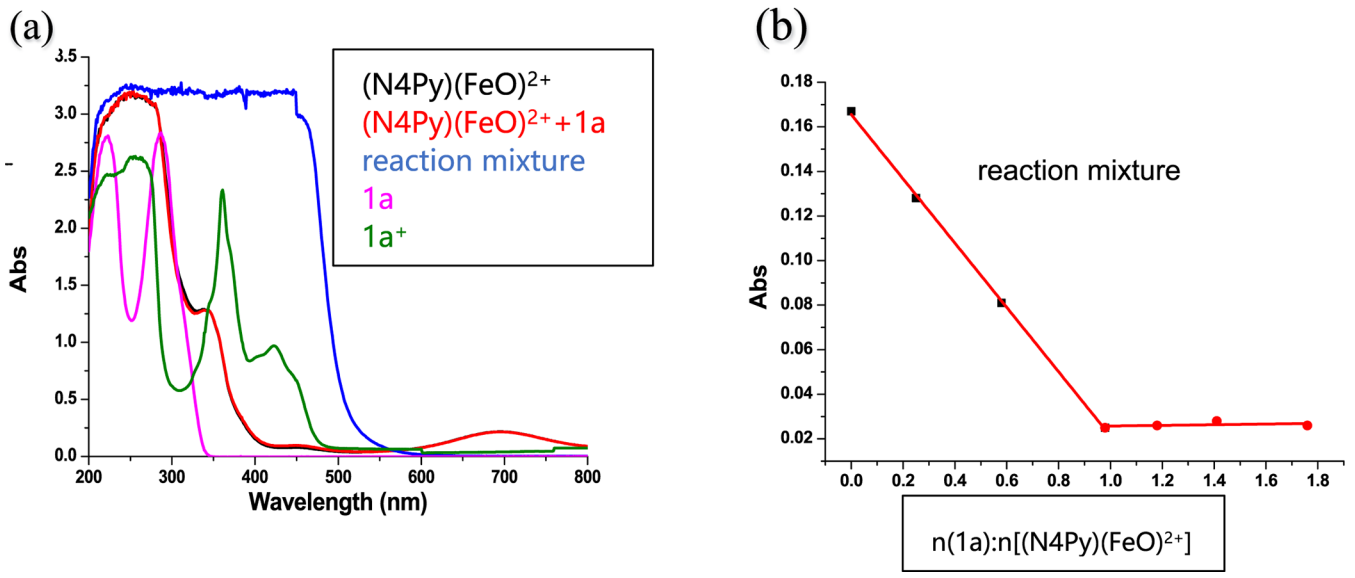

Figure 9. (a) UV−vis absorption spectrum of $(N4Py)(FeO)^{2+}(ClO_4)_2$, **1a**$^+$, and **1a**, mixtures of $(N4Py)(FeO)^{2+}(ClO_4)_2$, **1a** and CF_3COOH, and the product of the reaction between $(N4Py)(FeO)^{2+}$ and **1a** in the presence of CF_3COOH. The concentration of all compounds was 0.1 mM. (b) Linear fitting of the ultraviolet absorption of $(N4Py)(FeO)^{2+}(ClO_4)_2$ in the hydride transfer reaction from **1a** to $(N4Py)(FeO)^{2+}(ClO_4)_2$ in the presence of CF_3COOH (0.1 M).

electron transfer step (step 1) was less than 23.06 kcal/mol or not.

Second, the reaction in the thermodynamic platforms between $(N4Py)(FeO)^{2+}$ and **3** and between (Bn-TPEN)-$(FeO)^{2+}$ and **1a** followed step c or f, although step a had a considerably smaller value than that of step c. Hence, the thermodynamic advantage is not sufficient to determine the reaction mechanism. The energy difference owing to the molecular deformation of each compound from the initial to a transient state was defined as the deformation energy difference. Generally, the deformation energy difference owing to the release of hydride ions from each molecule is maximum. Therefore, it was deemed that the competition between the thermodynamic driving force difference and the deformation energy difference of the compounds in the two pathways determined the reaction mechanism.

(3) Can the reaction mechanism be changed by increasing the proton concentration? What are the external factors affecting the reaction mechanism?

Proton-coupled electron transfer plays a critical role in biological reactions and often involves metal complex enzymes, such as the oxidizing reaction in hydrogenase, the reaction of nitrogen fixation in dinitrogenase, the oxidation−reduction reaction in cytochrome c oxidase, and the preparation of O_2 from water in PSII. Only the molar absorbance at the maximum absorption wavelength of $(N4Py)(FeO)^{2+}$ was changed, but its chemical structure was barely changed for the long term in the presence of CF_3COOH. Therefore, the possibility of a new reaction mechanism between $(N4Py)(FeO)^{2+}$ and **1a** under acidic conditions was explored.

First, the UV−vis absorption spectra of $(N4Py)(FeO)^{2+}$, **1a**, and **1a**$^+$, the mixture of $(N4Py)(FeO)^{2+}$ and CF_3COOH, and the reaction product between $(N4Py)(FeO)^{2+}$ and **1a** (Figure 9a), the absorbance change in the reaction between (N4Py)-$(FeO)^{2+}$ and **1a** (Figure 9b), and the nuclear magnetic resonance test result of the product mixture (Supporting Information) showed a 1:1 stoichiometry.

Then, CV was used to test the reduction potential of $(N4Py)(FeO)^{2+}$ in the anhydrous acetonitrile solution with a concentration range of 0−2.0 M CF_3COOH (Supporting Information). The results showed that the reduction potential value moved in the positive direction with an increased CF_3COOH concentration.

Finally, it was inferred that the reaction might follow a multistep hydride anion transfer mechanism. The reduction potential value of $(N4Py)(FeO)^{2+}$ moved in the positive direction, and the energy barrier in the initial electron initiation step was reduced to 9.0 kcal/mol, which is lower than the energy barrier in the transition state. Additionally, adding O_2 profoundly affected the reaction rate. Therefore, these results supported the previously mentioned speculations.

If the reaction followed pathway a, then the apparent rate constant k_H^- would equal k_H. The reaction rate would be only relevant to the initial reactant concentration and irrelevant to the added acid concentration. These data disagree with the experimental phenomenon that the reaction rate is directly proportional to the acid concentration, excluding pathway a. If the reaction followed pathway b, the apparent rate constant k_H^- was equal to $k_p k_{et}/(k_p + k_{-et})$, and the KIE would be 1.37, indicating that the rate-determining step involved the C−H bond breakage. If $k_{p+} \ll k_{-et}$, $k_H^- = k_p k_{et}/k_{-et}$, and the H^+ concentration would affect the proton transfer rate. These data comply with the experimental phenomenon. If the reaction followed pathway c, the apparent rate constant k_H^- would be equal to $k_H' k_{et}/(k_H' + k_{-et})$, which was impossible for pathway a. Therefore, it was concluded that the reaction followed the e^-−H^+−e^- transfer mechanism (Figure 10, Scheme 6).

4. CONCLUSION

This study synthesized two mononuclear nonheme metal complexes and three series of organic hydride compounds to obtain the corresponding thermodynamic and reaction kinetic data and established the molecular IDs and chemical-reaction thermodynamic platforms of $(N4Py)(FeO)^{2+}$ and (Bn-TPEN)-$(FeO)^{2+}$. The following conclusions were drawn:

https://doi.org/10.1021/acsomega.4c08847
ACS Omega 2025, 10, 3718−3728

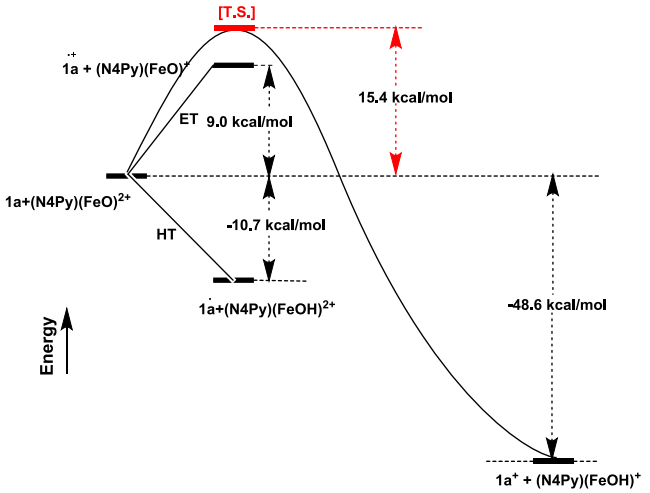

Figure 10. Comparison of state energy changes for the three possible initial steps with the activation free energy of the hydride transfer reaction between $(N4Py)(FeO)^{2+}$ and **1a** in the presence of CF_3COOH (0.1 M).

1. The thermodynamic data of the $(N4Py)(FeO)^{2+}$ and $(Bn\text{-}TPEN)(FeO)^{2+}$ molecules and the corresponding intermediates were obtained, providing a theoretical foundation for quantitatively analyzing their thermodynamic properties.

2. The reaction between $(N4Py)(FeO)^{2+}$ and **1**/**2** followed a one-step hydride anion transfer mechanism. The reactions between $(N4Py)(FeO)^{2+}$ and **3**, and between $(Bn\text{-}TPEN)(FeO)^{2+}$ and **1**, followed the hydrogen atom−electron transfer mechanism. The reaction between $(N4Py)(FeO)^{2+}$ and **1** followed the electron−proton−electron transfer mechanism under acidic conditions.

3. The internal factor affecting the reaction mechanism may be the competition between the thermodynamic driving force and the deformation energy differences of the molecules from the initial to a transient state. The external factor causing changes in the reaction mechanism and proton transfer rate was the addition of protons, triggering changes in the thermodynamic properties of the intermediate.

■ ASSOCIATED CONTENT

Supporting Information

Additional Supporting Information can be found in the online version of this article on the publisher's website. The Supporting Information is available free of charge at https://pubs.acs.org/doi/10.1021/acsomega.4c08847.

(PDF)

Scheme 6. Possible Mechanisms for Multiple-Step Hydride Transfer from 1 to $(N4Py)(FeO)^{2+}$ in the Presence of CF_3COOH (0.1 M)

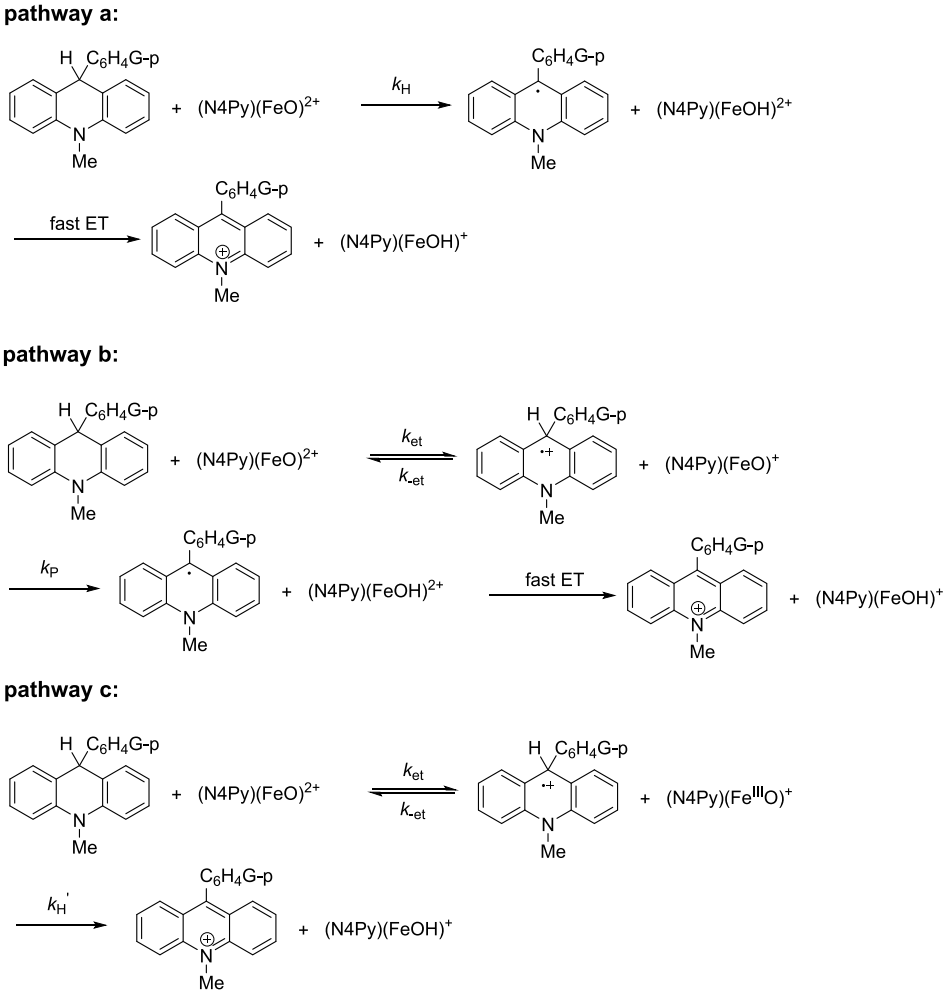

https://doi.org/10.1021/acsomega.4c08847
ACS Omega 2025, 10, 3718−3728

AUTHOR INFORMATION

Corresponding Authors

Bao-Long Chen − *The State Key Laboratory of Elemento-Organic Chemistry, Collaborative Innovation Center of Chemical Science and Engineering, College of Chemistry, Nankai University, Tianjin 300071, P. R. China;* Present Address: University of Nebraska Medical Center, College of Pharmacy, Department of Pharmaceutical Sciences, 42nd and Emile Streets, Omaha, NE 68198, United States; orcid.org/0009-0005-9589-5939; Email: baolongc116@gmail.com

Jin-Ye Zhang − *The State Key Laboratory of Elemento-Organic Chemistry, Collaborative Innovation Center of Chemical Science and Engineering, College of Chemistry, Nankai University, Tianjin 300071, P. R. China;* orcid.org/0000-0002-6028-2471; Email: zjynku@163.com

Xiao-Qing Zhu − *The State Key Laboratory of Elemento-Organic Chemistry, Collaborative Innovation Center of Chemical Science and Engineering, College of Chemistry, Nankai University, Tianjin 300071, P. R. China;* orcid.org/0000-0003-2785-640X; Email: xqzhu@nankai.edu.cn

Authors

Wen-Jie Xu − *The State Key Laboratory of Elemento-Organic Chemistry, Collaborative Innovation Center of Chemical Science and Engineering, College of Chemistry, Nankai University, Tianjin 300071, P. R. China*

Sheng-Yi Yan − *The State Key Laboratory of Elemento-Organic Chemistry, Collaborative Innovation Center of Chemical Science and Engineering, College of Chemistry, Nankai University, Tianjin 300071, P. R. China*

Complete contact information is available at: https://pubs.acs.org/10.1021/acsomega.4c08847

Notes

The authors declare no competing financial interest.

ACKNOWLEDGMENTS

Financial support from the National Natural Science Foundation of China (Grant Nos. 21672111, 21472099, 21390400, and 21102074) is gratefully acknowledged.

REFERENCES

(1) Solomon, E. I.; Brunold, T. C.; Davis, M. I.; Kemsley, J. N.; Lee, S. K.; Lehnert, N.; Neese, F.; Skulan, A. J.; Yang, Y. S.; Zhou, J. Geometric and electronic structure/function correlations in non-heme iron enzymes. *Chem. Rev.* **2000**, *100*, 235−350.

(2) Abu-Omar, M. M.; Loaiza, A.; Hontzeas, N. Reaction mechanisms of mononuclear non-heme iron oxygenases. *Chem. Rev.* **2005**, *105*, 2227−2252.

(3) Rohde, J. U.; In, J. H.; Lim, M. H.; Brennessel, W. W.; Bukowski, M. R.; Stubna, A.; Münck, E.; Nam, W.; Que, L. Jr Crystallographic and spectroscopic characterization of a Nonheme Fe(IV)═O complex. *Science* **2003**, *299*, 1037−1039.

(4) Klinker, E. J.; Kaizer, J.; Brennessel, W. W.; Woodrum, N. L.; Cramer, C. J.; Que, L. Jr Structures of nonheme oxoiron(IV) complexes from X-ray crystallography, NMR spectroscopy, and DFT calculations. *Angew. Chem., Int. Ed.* **2005**, *44*, 3690−3694.

(5) Shan, X.; Que, L., Jr High-valent nonheme iron-oxo species in biomimetic oxidations. *J. Inorg. Biochem.* **2006**, *100*, 421−433.

(6) Ekanayake, D. M.; Fischer, A. A.; Elwood, M. E.; Guzek, A. M.; Lindeman, S. V.; Popescu, C. V.; Fiedler, A. T. Nonheme iron−thiolate complexes as structural models of sulfoxide synthase active sites. *Dalton Trans.* **2020**, *49*, 17745−17757.

(7) Kaizer, J.; Klinker, E. J.; Oh, N. Y.; Rohde, J. U.; Song, W. J.; Stubna, A.; Kim, J.; Münck, E.; Nam, W.; Que, L. Jr Two-state reactivity in alkane hydroxylation by nonheme iron-oxo comolexes. *J. Am. Chem. Soc.* **2004**, *126*, 472−473.

(8) Sastri, C. V.; Sook Seo, M.; Joo Park, M.; Mook Kim, K.; Nam, W. Formation, stability, and reactivity of a mononuclear nonheme oxoiron(IV) complex in aqueous solution. *Chem. Commun.* **2005**, No. 11, 1405−1407.

(9) Chen, T.-Y.; Xue, S.; Tsai, W.-C.; Chien, T. C.; Guo, Y.-S.; Chang, W.-C. Deciphering pyrrolidine and olefin formation mechanism in kainic acid biosynthesis. *ACS Catal.* **2021**, *11*, 278−282.

(10) Oh, N. Y.; Suh, Y.; Park, M. J.; Seo, M. S.; Kim, J.; Nam, W. Mechanistic insight into alcohol oxidation by high-valent iron-oxo complexes of heme and nonheme ligands. *Angew. Chem., Int. Ed.* **2005**, *44*, 4235−4239.

(11) Bopp, C. E.; Kohler, H. E.; Hofstetter, T. B. Enzyme Kinetics of organic contaminant oxygenations. *Chimia* **2020**, *74*, 108−114.

(12) Sardar, S.; Weitz, A.; Hendrich, M. P.; Pierce, B. S. Outer-sphere tyrosine 159 within the 3-mercaptopropionic acid dioxygenase S-H-Y motif gates substrate-coordination denticity at the nonheme iron active site. *Biochemistry* **2019**, *58*, 5135−5150.

(13) Bukowski, M. R.; Koehntop, K. D.; Stubna, A.; Bominaar, E. L.; Halfen, J. A.; Münck, E.; Nam, W.; Que, L., Jr A thiolate-ligated nonheme oxoiron(IV) complex relevant to cytochrome P450. *Science* **2005**, *310*, 1000−1002.

(14) Sastri, C. V.; Oh, K.; Lee, Y. J.; Seo, M. S.; Shin, W.; Nam, W. Oxygen-atom transfer between mononuclear nonheme iron(IV)-oxo and iron(II) complexes. *Angew. Chem., Int. Ed.* **2006**, *45*, 3992−3995.

(15) Lu, J.-R.; Wang, B.-J.; Shaik, S.; Lai, W. QM/MM Calculations Reveal the Important Role of α-Heteroatom Substituents in Controlling Selectivity of Mononuclear Nonheme HppE-Catalyzed Reactions. *ACS Catal.* **2020**, *10*, 9521−9532.

(16) Nehru, K.; Seo, M. S.; Kim, J.; Nam, W. Oxidative N-dealkylation reactions by oxoiron(IV) complexes of nonheme and heme ligands. *Inorg. Chem.* **2007**, *46*, 293−298.

(17) Balland, V.; Charlot, M.-F.; Banse, F.; Girerd, J.-J.; Mattioli, T. A.; Bill, E.; Bartoli, J.-F.; Battioni, P.; Mansuy, D. Spectroscopic characterization of an Fe intermediate generated by reaction of XO (X = Cl, Br) with an Fe complex bearing a pentadentate non-porphyrinic ligand − Hydroxylation and epoxidation activity. *Eur. J. Inorg. Chem.* **2004**, *2004*, 301−308.

(18) Kripli, B.; Sólyom, B.; Speier, G.; Kaizer, J. Stability and catalase-like activity of a mononuclear non-heme Oxoiron(IV) complex in aqueous solution. *Molecules* **2019**, *24*, 3236.

(19) Zhu, X.-Q.; Liu, Q.-Y.; Chen, Q.; Mei, L.-R. Hydride, Hydrogen, Proton, and Electron Affinities of Imines and Their Reaction Intermediates in Acetonitrile and Construction of Thermodynamic Characteristic Graphs (TCGs) of Imines as a "Molecule ID Card. *J. Org. Chem.* **2010**, *75*, 789−808.

(20) Wayner, D. D. M.; Parker, V. D. Bond energies in solution from electrode potentials and thermochemical cycles. A simplified and general approach. *Acc. Chem. Res.* **1993**, *26*, 287−294.

(21) Osteryoung, J. G.; Osteryoung, R. A. Square Wave Voltammetrv. *Anal. Chem.* **1985**, *57* (1), 101−110.

(22) Espinoza, E. M.; Clark, J. A.; Soliman, J.; Derr, J. B.; Morales, M.; Vullev, V. I. Practical Aspects of Cyclic Voltammetry: How to Estimate Reduction Potentials When Irreversibility Prevails. *J. Electrochem. Soc.* **2019**, *116*, H3175−H3187.

(23) Zhu, X. Q.; Zhang, M. T.; Yu, A.; Wang, C. H.; Cheng, J. P. Hydride, hydrogen atom, proton and electron transfer driving forces of various five-membered heterocyclic organic hydrides and their reaction intermediates in acetonitrile. *J. Am. Chem. Soc.* **2008**, *130*, 2501−2516.

(24) Zhu, X. Q.; Dai, Z.; Yu, A.; Wu, S.; Cheng, J. P. Driving forces for the mutual conversions between phenothiazines and their various reaction intermediates in acetonitrile. *J. Phys. Chem. B* **2008**, *112*, 11694−11707.

(25) Zhu, X. Q.; Tan, Y.; Cao, C. T. Thermodynamic diagnosis of the properties and mechanism of dihydropyridine-type compounds as hydride source in acetonitrile with "molecule ID card. *J. Phys. Chem. B* **2010**, *114*, 2058−2075.
(26) Arnett, E. M.; Amarnath, K.; Harvey, N. G.; Cheng, J.-P. Determination and interrelation of bond heterolysis and homolysis energies in solution. *J. Am. Chem. Soc.* **1990**, *112*, 344−355.
(27) Chen, B. L.; Yan, S. Y.; Zhu, X. Q. A Mechanism study of redox reactions of the ruthenium-oxo-polypyridyl complex. *Molecules* **2023**, *28*, 4401.

https://doi.org/10.1021/acsomega.4c08847
ACS Omega 2025, 10, 3718−3728